The Astrophysical Journal, 889:54 (5pp), 2020 January 20 https://doi.org/10.3847/1538-4357/ab5e87

An Apparently Eccentric Orbit of the Exoplanet WASP-12 b as a Radial Velocity Signature of Planetary-induced Tides in the Host Star

Gracjan Maciejewski[1], Andrzej Niedzielski[1], Eva Villaver[2], Maciej Konacki[3], and Rafał K. Pawłaszek[3]
[1] Institute of Astronomy, Faculty of Physics, Astronomy and Informatics, Nicolaus Copernicus University, ul. Grudziadzka 5, 87-100 Toruń, Poland; gmac@umk.pl
[2] Departamento de Física Teórica, Universidad Autónoma de Madrid, Cantoblanco E-28049 Madrid, Spain
[3] Nicolaus Copernicus Astronomical Center, Department of Astrophysics, ul. Rabiańska 8, 87–100 Toruń, Poland
Received 2019 November 20; revised 2019 November 28; accepted 2019 December 2; published 2020 January 24

Abstract

Massive exoplanets on extremely tight orbits, such as WASP-12 b, induce equilibrium tides in their host stars. Following the orbital motion of the planet, the tidal fluid flow in the star can be detected with the radial velocity method. Its signature manifests as the second harmonics of the orbital frequency that mimics a nonzero orbital eccentricity. Using the new radial velocity measurements acquired with the HARPS-N spectrograph at the Telescopio Nazionale Galileo and combining them with the literature data, we show that the apparent eccentricity of WASP-12 b's orbit is nonzero at a 5.8σ level, and the longitude of periastron of this apparently eccentric orbit is close to 270°. This orbital configuration is compatible with a model composed of a circular orbit and a signature of tides raised in the host star. The radial velocity amplitude of those tides was found to be consistent with the equilibrium tide approximation. The tidal deformation is predicted to produce a flux modulation with an amplitude of 80 ppm that could be detected using space-borne facilities.

Unified Astronomy Thesaurus concepts: Hot Jupiters (753); Radial velocity (1332); Exoplanet tides (497)

1. Introduction

The WASP-12 system belongs to a small group of planetary systems with giant planets on extremely tight orbits. The late F-type host star is orbited by the bloated hot Jupiter WASP-12 b with an orbital period $P_{\rm orb}$ of about 1.09 days (Hebb et al. 2009). The proximity of the host star (i.e., 0.023 au or about 3 stellar radii) results in an equilibrium temperature of the order of 2500 K. This unique system architecture has given rise to a number of studies on the planetary atmosphere and planet–star interactions (see Haswell 2017 for a comprehensive review). The planet was found to be surrounded by a translucent exosphere producing strong absorption by resonance lines of metals in the near-UV (Fossati et al. 2010). The exospheric gas overfills the Roche lobe and the planet is losing mass via both the Lagrangian L1 and L2 points. Numerical simulations show that the gaseous envelope forms a circumstellar disk (Debrecht et al. 2018).

Maciejewski et al. (2016) detected apparent shortening of the orbital period that could be caused by shrinking of the orbit due to tidal decay or could be a part of the long-term periodic variations produced by apsidal precession. Apsidal precession was found to be disfavored by new transit and occultation timing (Patra et al. 2017; Maciejewski et al. 2018; Yee et al. 2020) and gives an upper limit for the orbital eccentricity $e_{\rm b}$ of the order of 10^{-3} (Maciejewski et al. 2016; Patra et al. 2017). Such a small value is not surprising because the planetary orbit is expected to be circularized on a relative short timescale due to efficient dissipation of planetary tides. The rate of the tidal decay is related to the modified tidal quality factor Q'_*, which parameterizes the response of the star's interior to tidal perturbation induced by a planet. For the WASP-12 system, the value of Q'_* was found to be of the order of 10^5 (Maciejewski et al. 2016, 2018; Patra et al. 2017; Yee et al. 2020) that is 1–2 orders of magnitude lower than the typical values obtained from studies of binary stars (e.g., Meibom & Mathieu 2005) and other planetary systems (e.g., Bonomo et al. 2017). As discussed by Bailey & Goodman (2019), the nature of this discrepancy remains unresolved.

Using the equilibrium tide approximation, Arras et al. (2012) showed that tides, which are risen by a massive planet in its host star, could be detected with the radial velocity (RV) method. These tidal deformations of the star are expected to manifest themselves in the form of an RV signal with an amplitude of a few m s^{-1}. The period of this signal is half of the orbital period and its phase is related to the planetary orbital motion in such a way that the RV signature of tides can be mimicked by an apparently nonzero orbital eccentricity and a longitude of periastron equal to 270°. In this study, we demonstrate that these conditions are met in the WASP-12 system.

2. Observational Data

2.1. New RV Observations

We acquired 17 RV measurements with the High Accuracy RV Planet Searcher in the northern hemisphere (HARPS-N; Cosentino et al. 2012) fed by the 3.58 m Telescopio Nazionale Galileo (TNG), located at the Observatorio del Roque de los Muchachos on La Palma (Spain). The instrument is an echelle spectrograph covering the wavelength range between 383 and 693 nm with a maximal resolving power of $R = 115{,}000$. Spectra were gathered between 2013 January 2 and 2017 November 16, most of them as a backup of the Tracking Advance Planetary Systems (TAPAS) project (Niedzielski et al. 2015; Villaver et al. 2017). The standard user pipeline, which is based on the weighted cross-correlation function method, was used to reduce the data and to determine the high-precision RV measurements and their uncertainties. The simultaneous Th–Ar calibration mode of the spectrograph was used for wavelength calibration. The G2 cross-correlation mask, which is the closest to the spectral type of WASP-12, was used to determine RVs. The details on individual observations are given in Table 1.

Table 1
Individual Doppler Observations

UT Start	t_{exp} (s)	X	d_{Moon} (°)	BJD_{TDB}	RV (km s^{-1})	σ_{RV} (km s^{-1})
2013 Jan 2, 02:54:44	1605	1.14 → 1.22	59.8	2456294.637014	18.9829	0.0028
2013 Jan 28, 23:59:50	1458	1.03 → 1.06	55.3	2456321.513859	19.3190	0.0033
2013 Mar 22, 22:58:20	1949	1.44 → 1.66	33.6	2456374.469642	18.8632	0.0033
2013 Apr 28, 21:10:47	2202	1.73 → 2.14	162.6	2456411.392928	19.0165	0.0031
2013 Dec 9, 03:03:08	1500	1.01 → 1.04	115.9	2456635.641731	19.1406	0.0105
2013 Dec 20, 23:29:26	1288	1.12 → 1.08	34.3	2456647.492182	18.9412	0.0055
2013 Dec 21, 04:46:35	1442	1.35 → 1.47	35.9	2456647.713618	19.2107	0.0044
2014 Jan 27, 19:33:06	1605	1.42 → 1.29	163.6	2456685.329266	19.0232	0.0095
2014 Jan 28, 00:35:28	1481	1.07 → 1.11	166.4	2456685.539009	18.8710	0.0045
2014 Mar 23, 21:29:52	1904	1.13 → 1.21	168.0	2456740.407717	19.1097	0.0033
2014 Apr 8, 20:56:10	1800	1.20 → 1.31	31.1	2456756.381790	18.9077	0.0040
2014 Apr 9, 22:02:54	1800	1.51 → 1.74	42.7	2456757.427242	18.9604	0.0161
2014 Apr 11, 21:38:47	1800	1.43 → 1.62	66.3	2456759.411696	19.1810	0.0073
2014 Apr 22, 20:51:41	1852	1.34 → 1.50	144.9	2456770.367480	19.1278	0.0024
2015 Feb 12, 23:01:28	500	1.02 → 1.02	145.6	2457066.463996	18.8624	0.0102
2015 Apr 22, 21:00:29	2206	1.37 → 1.59	16.5	2457135.373626	18.9487	0.0037
2017 Nov 16, 03:38:31	1187	1.01 → 1.00	110.9	2458073.663121	18.9540	0.0042

Note. UT start is the date of the beginning of the exposure. t_{exp} is the exposure time. X shows the airmass change during the exposure. d_{Moon} is the angular distance of the Moon at the middle of the exposure. BJD_{TDB} is barycentric Julian date in barycentric dynamical time of the exposure centroid. RV and σ_{RV} are the determined values of radial velocity and its uncertainty, respectively.

2.2. Literature Data

We used the RV measurements from Hebb et al. (2009) and Husnoo et al. (2011). They were acquired with the SOPHIE spectrometer (Perruchot et al. 2008) and the 1.9 m telescope at the Observatoire de Haute Provence (France) in the observing seasons 2007/2008, 2008/2009, and 2009/2010. Since Husnoo et al. (2011) note that the velocity zero-point floats by several dozen m s^{-1} in a timescale of several months, the data set was split into three subsets for the individuals seasons each.

Precise Doppler measurements were extracted from Knutson et al. (2014), including reprocessed observations originally used by Albrecht et al. (2012). That survey was performed with the High Resolution Echelle Spectrometer (HIRES; Vogt et al. 1994) coupled with the 10 m Keck I telescope between 2009 and 2013.

Additional data obtained with HARPS-N were taken from Bonomo et al. (2017). Those precise observations were performed within a framework of the Global Architecture of Planetary Systems (GAPS) Consortium (Poretti et al. 2016) between 2012 and 2015.

2.3. Data Preprocessing

In the data set acquired with SOPHIE in the observing season 2008/2009, three measurements have errors 2–3 times greater than the remaining measurements. They were identified as outliers in our preliminary analysis. As discussed by Maciejewski et al. (2013), those measurements were likely affected by clouds and therefore they were skipped in the final iteration.

Since our procedure does not take the Rossiter–McLaughlin (RM) effect into account and some RV measurements were performed when the planet was transiting, the RM signature was subtracted from those measurements. The appropriate corrections of up to 11.4 m s^{-1} were calculated using a model of the RM effect obtained by Albrecht et al. (2012).

The RV jitter is often equated with RV noise produced by stellar intrinsic variability that is caused by convection motions in the stellar envelope and photospherical inhomogeneities (Wright 2005) or solar-like acoustic waves (Bedding & Kjeldsen 2007). In practice, it is determined as an additional uncertainty that must be added in quadrature to the RV errors in order to obtain a reduced chi-square statistic of unity for an assumed model. Therefore, this quantity may contain not only the physical stellar jitter, but also variations from still-undetected planets and components of instrumental and methodological origin (Isaacson & Fischer 2010; Meunier & Lagrange 2019). The stellar jitter for WASP-12 was found to be equal to $9.1^{+1.8}_{-1.3}$ m s^{-1} by Bonomo et al. (2017), who used all RV measurements available then and treated jitter as a free parameter while fitting an orbital solution. We noticed, however, that in the case of WASP-12 the jitter is reduced if lower-quality data are iteratively rejected. The value of jitter stabilized at ∼7.4 m s^{-1} for the RV measurements with the errors below 8 m s^{-1}. A single-night estimate of the jitter, determined for a high-precision Doppler time series acquired on 2012 January 1/2 by Albrecht et al. (2012), yields a value of 4.8 m s^{-1}. This is de facto a lower constraint on stellar jitter because it does not account for stellar intrinsic variability in timescales longer than a couple of hours. The jitter value of ∼7.4 m s^{-1} represents variations on timescales of years and is greater than the single-night estimate by a factor of ∼1.5. This is in line with the finding reported by Brems et al. (2019) that the ratio of long- and short-timescale jitter is 1.5–1.7 for Gyr old stars. Considering the above, we used the jitter value of 7.4 m s^{-1} in further analysis. We note that using the single-night estimate of the jitter or the conservative value from Bonomo et al. (2017) does not change our quantitative conclusions.

3. Results

3.1. Orbital Eccentricity

A circular-orbit model is characterized by eight free parameters: an orbital period P_{orb}, RV amplitude K, mean anomaly for a given epoch M, and five zero-point RV levels for

individual data sets each. In addition, the orbital decay rate was included in the model with the decay rate characterized by the change in the orbital period between succeeding transits $\frac{dP_{\rm orb}}{dE} = (-9.67 \pm 0.73) \times 10^{-10}$ days per epoch^2 as refined by Maciejewski et al. (2018). The best-fitting solution was found with the Levenberg–Marquardt algorithm. The uncertainties of the parameters were determined with the bootstrap method using 10^5 resampled data sets. The minimizing procedure results in $(\chi^2_{\rm RV})_{\rm circ} = 186.0$ at 124 degrees of freedom.

The fitting procedure was repeated for a scenario allowing a nonzero eccentricity. Two additional parameters, the orbital eccentricity $e_{\rm orb}$ and longitude of periastron ω, were used to parameterize the shape and orientation of the orbit. The 10-parameter model gives $(\chi^2_{\rm RV})_{\rm ecc} = 142.5$ at 122 degrees of freedom.

To compare both models, the Bayesian information criterion (BIC) was calculated for each of them following the form

$$\mathrm{BIC} = \chi^2_{\rm RV} + k \ln N, \quad (1)$$

where k is the number of fit parameters and N is the number of data points. The criterion favors the eccentric-orbit model ($\mathrm{BIC_{ecc}} = 291.9$) over the circular-orbit model ($\mathrm{BIC_{circ}} = 304.8$) with a probability ratio of $e^{\Delta \mathrm{BIC}/2} = 6.2 \times 10^2$. We notice that the eccentric-orbit model is favored over the circular-orbit model even if a higher or lower value of stellar jitter is used. For instance, repeating the procedure with the conservative value of jitter of 9.1 m s^{-1} (Bonomo et al. 2017) results in the probability ratio of 1.5×10^2.

The best-fitting model gives $e_{\rm orb} = 0.035 \pm 0.006$ and $\omega = 270\overset{\circ}{.}7 \pm 0\overset{\circ}{.}6$. This is a 5.8σ detection of the non-circular orbit. Its orientation is consistent within a 1.2σ level with a specific way that is degenerated with the tidal RV signal.

3.2. Tidal Velocity

As shown by Arras et al. (2012), an apparently eccentric orbit may be de facto a sum of the first harmonic of the orbital frequency and the second harmonic associated with the tidal velocity. To construct a model with the tidal velocity component, the RV data sets were phase folded taking the effect of orbital period shortening into account. The barycentric velocity was subtracted but its contribution to the error budget was taken into account by introducing a parameter γ' that allows for corrections of the barycentric velocity. The phased RV signal $V_{\rm rad}$ was modeled with the formula

$$V_{\rm rad} = \gamma' + V_{\rm orb} + V_{\rm tide}, \quad (2)$$

where

$$V_{\rm orb} = -K_{\rm orb} \sin(2\pi(\phi - \phi_0) \quad (3)$$

is the orbital motion component (the first harmonic of the orbital frequency) and

$$V_{\rm tide} = K_{\rm tide} \sin(4\pi(\phi - \phi_0) \quad (4)$$

is the tidal velocity component (the second harmonic of the orbital frequency). The parameters $K_{\rm orb}$ and $K_{\rm tide}$ are the amplitudes, and ϕ_0 is the phase offset. The Markov Chain Monte Carlo algorithm was used to find the best-fitting parameters and their uncertainties. The posterior probability distributions were generated using 100 chains, each of which was 10^4 trials long after discarding the first 1000 steps. The best-fitting parameters were determined as the median values of marginalized posteriori probability distributions, and 15.9 and 84.1 percentile values of the cumulative distributions were used as 1σ uncertainties.

We obtained $K_{\rm orb} = 220.0 \pm 1.3$ m s^{-1} and $K_{\rm tide} = 7.5 \pm 1.2$ m s^{-1}. The parameters γ' with a value of -0.34 ± 0.82 m s^{-1} and ϕ_0 with a value of $(1.0^{+0.7}_{-0.8}) \times 10^{-3}$ were found to be consistent with zero well within 1σ and 2σ, respectively. The best-fitting model together with the orbital and tidal RV components and the residuals is shown in Figure 1.

4. Discussion

Preliminary detections of the nonzero eccentricity of WASP-12 b were reported in previous studies with lower significance. In the discovery paper, Hebb et al. (2009) found $e_{\rm orb} = 0.049 \pm 0.015$, Knutson et al. (2014) reported $e_{\rm orb} = 0.037^{+0.014}_{-0.015}$, and more recently Yee et al. (2020) obtained $e_{\rm orb} = 0.0317 \pm 0.0087$. In all those studies, the reported values of ω were close to 270°, and Yee et al. (2020) pointed out the tidal distortion of the host star as a possible explanation of this specific configuration. On the other hand, Husnoo et al. (2011) found $e_{\rm orb} = 0.018^{+0.024}_{-0.014}$ that was interpreted as a result speaking in favor of a circular orbit. The same conclusion was reached by Bonomo et al. (2017), who placed a 1σ upper constraint on $e_{\rm orb}$ of 0.02.

Following Equation (3) in Adams & Laughlin (2006) and using a conservative value of the planetary quality factor of 10^6, the circularization timescale for WASP-12 b is about 0.4 Myr. This is much shorter than the system age that is estimated to be 4 orders of magnitude longer. If WASP-12's orbital eccentricity of ∼0.035 were real, an efficient mechanism that excites and sustains it would be needed to operate in the system. Bailey & Goodman (2019) consider perturbations from undetected planetary companion, Kozai–Lidov oscillations, or fluctuations of the gravitational potential induced by stellar convection. The first two of those scenarios may be discarded because no perturbing body has been detected in the system. The magnitude of the third mechanism was found to be negligible. Furthermore, the orbit of WASP-12 b is expected to precess with a period of a few decades. This precession with $e_{\rm orb}$ of ∼0.035 would produce anticorrelated variations in transit and occultation times with amplitudes of ∼20 minutes. No evidence for such a scenario was found in timing observations (Patra et al. 2017; Yee et al. 2020). From this perspective, the tidal fluid flow is a natural explanation for the apparent nonzero eccentricity of WASP-12 b.

In the equilibrium tide approximation, stellar matter is assumed to be incompressible and to follow gravitational equipotentials ignoring fluid inertia. Furthermore, the forcing frequency is set to zero, any effects induced by convective motions are neglected, and the stellar rotation is set to zero. These simplifications make predictions of the equilibrium tide approximation to be accurate to a factor of ∼2 (Arras et al. 2012). In this context, our determination of the amplitude of the tidal velocity component $K_{\rm tide} = 7.3 \pm 0.8$ m s^{-1} can be considered as being consistent with the value of 4.78 m s^{-1} calculated under the equilibrium tide approximation (Arras et al. 2012).

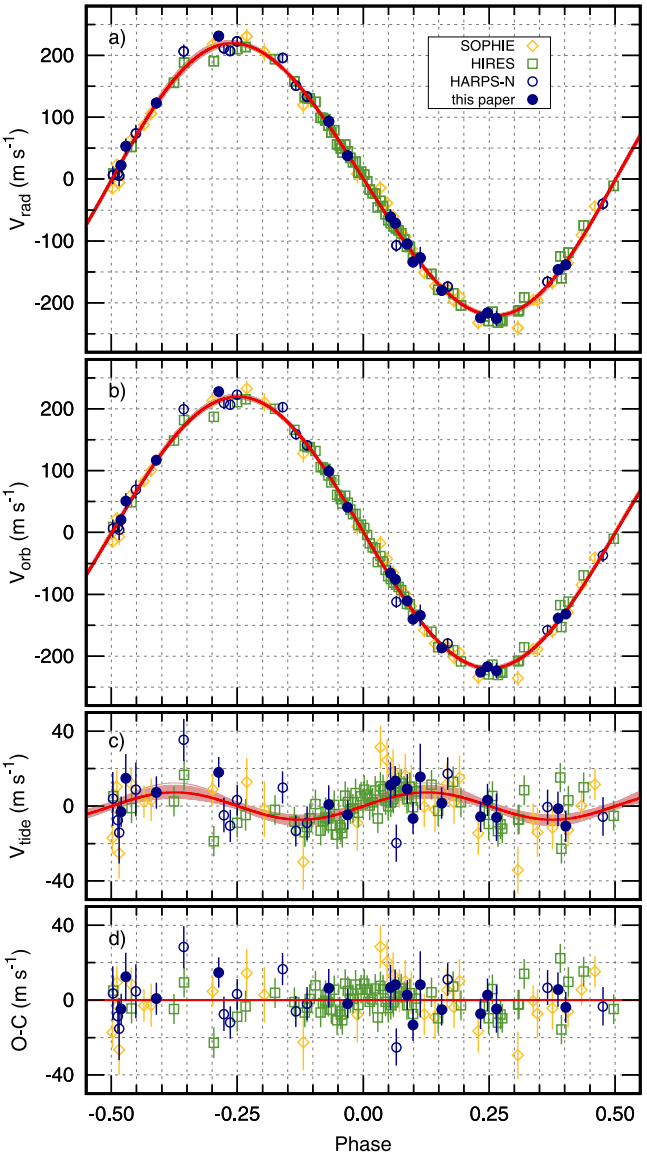

Figure 1. Panel (a): phase-folded RV curve for WASP-12 b with the apparently nonzero eccentricity. Our new observations are marked with dots and the literature data are marked with open symbols. The original errors are increased by the value of jitter of 7.4 m s^{-1} added in quadrature. The best-fitting model is marked with a red line. The parameter uncertainties of the model are illustrated with pale-red lines that are drawn for 50 sets of parameters, randomly chosen from the Markov chains. Panel (b): orbital RV component. Panel (c): tidal RV component that mimic the nonzero orbital eccentricity of WASP-12 b. Panel (d): the residuals from the best-fitting model.

The WASP-18 system was identified as the best candidate for detection of the tidal velocity (Arras et al. 2012). The amplitude of the tidal RV signal, predicted by the the equilibrium tide approximation, is $\sim$32 m s^{-1}. According to Bonomo et al. (2017), the orbital eccentricity of WASP-18 b is definitely nonzero with a value of 0.0076 $\pm$ 0.0010, and the pericenter longitude of $268.7^{+2.7}_{-2.9}$ degrees agrees with 270° well within a 1σ range. Such configuration corresponds to the tidal RV signal with an amplitude of $\sim$14 m s^{-1} that, though noticeably smaller, is still not far from the model predictions.

To verify a reliability of our procedure, we reanalyzed the data available for the WASP-18 system and compared the outcome to the results reported by Bonomo et al. (2017). We used the RV measurements from Triaud et al. (2010), including observations reported by Hellier et al. (2009), and from Knutson et al. (2014). The observations acquired during a transit phase were skipped leaving 53 data points for further analysis—the same data set that was analyzed in the original study. To place additional constraints on a transit ephemeris, we used all ground-based-transit mid-transit times that were published prior to the study of Bonomo et al. (2017), as compiled by Wilkins et al. (2017). Following the procedure that we applied to the WASP-12 system, we found that the WASP-18 b's eccentricity is 0.0082 $\pm$ 0.0010 and the longitude of periastron is 266°.1 $\pm$ 3°.3. Both quantities agree with the values reported by Bonomo et al. (2017) well within a 1σ range. The parameter uncertainties were found to be comparable with each other, which ensures that our procedure does not underestimates uncertainties. This finding strengthens the high detection significance of the nonzero apparent eccentricity for WASP-12 b.

For WASP-12, the tidal amplitude of 7.3 m s^{-1} corresponds to the height of tides up to $\sim$150 km. Such ellipsoidal deformation is predicted to produce a photometric modulation with an amplitude of $\sim$80 ppm. Such signals have been detected in the HAT-P-7 and WASP-18 systems using photometric time series from space-borne telescopes (Welsh et al. 2010; Shporer et al. 2019). Because of the relative faintness of the host star ($V = 11.7$ mag), the ellipsoidal flux modulation in the WASP-12 system would be possible with such instruments as TESS (Ricker et al. 2014) or CHEOPS (Broeg et al. 2013).

5. Conclusions

Massive planets on extremely tight orbits induce tidal deformations of their host stars that can be accessible not only by ultra-precise photometric observations, but also by the RV method. We have found that the orbit of WASP-12 b, like the orbit of WASP-18 b, appears to be apparently eccentric with the periastron longitude close to 270°. This is the RV manifestation of the tidal deformation of the host star that follows the orbital motion of the planet. Although the observations are considered as being consistent with predictions of the equilibrium tide approach, development of more advanced models would benefit our better understanding of planet–star tidal interactions.

We thank the anonymous referee for a prompt and insightful report. G.M. and A.N. acknowledge the financial support from the National Science Centre, Poland through grant No. 2016/23/B/ST9/00579. A.N. is also supported by the National Science Centre, Poland through grant No. 2015/19/B/ST9/02937. E.V. acknowledges support from the Spanish Ministerio de Ciencia, Innovación y Universidades under the project PGC2018-101950-B-I00. M.K. is supported by the Polish National Science Center (NCN) through grant 2017/27/B/ST9/02727.

Facility: TNG(HARPS-N).

ORCID iDs

Gracjan Maciejewski https://orcid.org/0000-0002-4195-5781
Andrzej Niedzielski https://orcid.org/0000-0002-0587-8854
Eva Villaver https://orcid.org/0000-0003-4936-9418

References

Adams, F. C., & Laughlin, G. 2006, ApJ, 649, 1004
Albrecht, S., Winn, J. N., Johnson, J. A., et al. 2012, ApJ, 757, 18

Arras, P., Burkart, J., Quataert, E., & Weinberg, N. N. 2012, MNRAS, 422, 1761
Bailey, A., & Goodman, J. 2019, MNRAS, 482, 1872
Bedding, T. R., & Kjeldsen, H. 2007, CoAst, 150, 106
Bonomo, A. S., Desidera, S., Benatti, S., et al. 2017, A&A, 602, A107
Brems, S. S., Kürster, M., Trifonov, T., Reffert, S., & Quirrenbach, A. 2019, A&A, 632, A37
Broeg, C., Fortier, A., Ehrenreich, D., et al. 2013, EPJWC, 47, 03005
Cosentino, R., Lovis, C., Pepe, F., et al. 2012, Proc. SPIE, 8446, 84461V
Debrecht, A., Carroll-Nellenback, J., Frank, A., et al. 2018, MNRAS, 478, 2592
Fossati, L., Haswell, C. A., Froning, C. S., et al. 2010, ApJL, 714, L222
Haswell, C. A. 2017, in Handbook of Exoplanets, ed. H. Deeg & J. Belmonte (Cham: Springer), 1
Hebb, L., Collier-Cameron, A., Loeillet, B., et al. 2009, ApJ, 693, 1920
Hellier, C., Anderson, D. R., Collier Cameron, A., et al. 2009, Natur, 460, 1098
Husnoo, N., Pont, F., Hébrard, G., et al. 2011, MNRAS, 413, 2500
Isaacson, H., & Fischer, D. 2010, ApJ, 725, 875
Knutson, H. A., Fulton, B. J., Montet, B. T., et al. 2014, ApJ, 785, 126
Maciejewski, G., Dimitrov, D., Fernández, M., et al. 2016, A&A, 588, L6
Maciejewski, G., Dimitrov, D., Seeliger, M., et al. 2013, A&A, 551, A108
Maciejewski, G., Fernández, M., Aceituno, F., et al. 2018, AcA, 68, 371
Meibom, S., & Mathieu, R. D. 2005, ApJ, 620, 970
Meunier, N., & Lagrange, A. M. 2019, A&A, 628, A125
Niedzielski, A., Villaver, E., Wolszczan, A., et al. 2015, A&A, 573, A36
Patra, K. C., Winn, J. N., Holman, M. J., et al. 2017, AJ, 154, 4
Perruchot, S., Kohler, D., Bouchy, F., et al. 2008, Proc. SPIE, 7014, 70140J
Poretti, E., Boccato, C., Claudi, R., et al. 2016, MmSAI, 87, 141
Ricker, G. R., Winn, J. N., Vanderspek, R., et al. 2014, Proc. SPIE, 9143, 914320
Shporer, A., Wong, I., Huang, C. X., et al. 2019, AJ, 157, 178
Triaud, A. H. M. J., Collier Cameron, A., Queloz, D., et al. 2010, A&A, 524, A25
Villaver, E., Niedzielski, A., Wolszczan, A., et al. 2017, A&A, 606, A38
Vogt, S. S., Allen, S. L., Bigelow, B. C., et al. 1994, Proc. SPIE, 2198, 362
Welsh, W. F., Orosz, J. A., Seager, S., et al. 2010, ApJL, 713, L145
Wilkins, A. N., Delrez, L., Barker, A. J., et al. 2017, ApJL, 836, L24
Wright, J. T. 2005, PASP, 117, 657
Yee, S. W., Winn, J. N., Knutson, H. A., et al. 2020, ApJL, 888, L5